

## University of New Hampshire University of New Hampshire Scholars' Repository

---

Center for Coastal and Ocean Mapping

Center for Coastal and Ocean Mapping

---

4-2014

# Pose Detection and control of multiple unmanned underwater vehicles using optical feedback

Firat Eren

*University of New Hampshire, Durham, [Firat.Eren@unh.edu](mailto:Firat.Eren@unh.edu)*

Shachak Pe'eri

*University of New Hampshire, Durham, [shachak.peeri@unh.edu](mailto:shachak.peeri@unh.edu)*

Yuri Rzhanov

*University of New Hampshire, Durham, [Yuri.Rzhanov@unh.edu](mailto:Yuri.Rzhanov@unh.edu)*


May-Win Thein

*University of New Hampshire, Durham*

Barbaros Celikkol

*University of New Hampshire, Durham*

Follow this and additional works at: <https://scholars.unh.edu/ccom>

 Part of the [Computer Sciences Commons](#), and the [Oceanography and Atmospheric Sciences and Meteorology Commons](#)

---

### Recommended Citation

F. Eren, Pe'eri, S., Rzhanov, Y., Thein, M. - W., and Celikkol, B., "Pose Detection and control of multiple unmanned underwater vehicles using optical feedback", Oceans '14 MTS/IEEE. Taipei, Tawian, 2014.

This Conference Proceeding is brought to you for free and open access by the Center for Coastal and Ocean Mapping at University of New Hampshire Scholars' Repository. It has been accepted for inclusion in Center for Coastal and Ocean Mapping by an authorized administrator of University of New Hampshire Scholars' Repository. For more information, please contact [nicole.hentz@unh.edu](mailto:nicole.hentz@unh.edu).

# Pose Detection and Control of Multiple Unmanned Underwater Vehicles (UUVs) Using Optical Feedback

Firat Eren, May-Win Thein, Shachak Pe'eri, Yuri Rzhanov, Barbaros Celikkol and Robinson Swift  
 University of New Hampshire  
 fob2@unh.edu, mthein@cisunix.unh.edu, shachak@ccom.unh.edu, yuri.rzhanov@unh.edu, celikkol@unh.edu,  
 mrsswift@cisunix.unh.edu

**Abstract**— This paper proposes pose detection and control algorithms in order to control the relative pose between two Unmanned Underwater Vehicles (UUVs) using optical feedback. The leader UUV is configured to have a light source at its crest which acts as a guiding beacon for the follower UUV which has a detector array at its bow. Pose detection algorithms are developed based on a classifier, such as the Spectral Angle Mapper (SAM), and chosen image parameters. An archive look-up table is constructed for varying combinations of 5-degree-of-freedom (DOF) motion (i.e., translation along all three coordinate axes as well as pitch and yaw rotations). Leader and follower vehicles are simulated for a case in which the leader is directed to specific waypoints in horizontal plane and the follower is required to maintain a fixed distance from the leader UUV. Proportional-Derivative (PD) control (without loss of generality) is applied to maintain stability of the UUVs to show proof of concept. Preliminary results indicate that the follower UUV is able to maintain its fixed distance relative to the leader UUV to within a reasonable accuracy.

**Keywords**- Unmanned underwater vehicle, optical feedback, leader-follower, detection, control design

## I. INTRODUCTION

Autonomous unmanned vehicles have been extensively used in tasks that are difficult and/or dangerous for the humans to accomplish. The unmanned vehicles are employed in space and air, on ground, and in underwater operations. In recent decades, there has been an increased interest in the coordinated control of multiple unmanned vehicles in order to reduce operational time and costs. One particular example is the use of multiple unmanned underwater vehicles (UUVs) in surveys [1-4]. This concept can be beneficial in large fleet surveys, as multiple vehicles are able to scan larger areas in less time, thus reducing operational costs.

For coordinated formation control of unmanned vehicles, a variety of architectures and strategies have been developed. The strategies used are mainly virtual structure, behavior based, leader-follower, artificial potential and graph theory [5]. In this paper the leader-follower strategy is used to evaluate formation control in underwater conditions. The leader-follower method is considered less complex than that of other approaches and considered reliable [6]. However, disadvantage of this method lies in the lack of communication from the followers to the leader.

A key requirement for the leader-follower method is the establishment of a communication link between the two UUVs. The challenge for underwater communications

arises from the fact that technologies that have been used for aerial and ground vehicles, e.g. GPS and radio signals, attenuate significantly and thus cannot be used in underwater applications. Recent studies on formation control of multiple UUVs in a leader-follower strategy mostly focus on acoustics as the method of communication between the vehicles [7-10]. While acoustic communication can be established over long distances, the hardware is often costly and the operational bandwidth is limited. Optical communication is a cost-effective alternative to acoustical detection as commercial-of-the-shelf (COTS) components are currently available that would sufficiently fit this proposed application. However, the effective communication range is shorter than that of acoustics. In addition, the optical properties of water constantly change and add to the process uncertainty.

Currently, the use of optical communication for UUV motion is limited. Current studies focus mainly on planar optical arrays for autonomous underwater vehicle (AUV) communication that include the use of a photodiode arrays to estimate AUV orientation to a light beacon [11], and the development of distance-detection algorithms for UUVs [12, 13]. Similar optical communication approaches were also used for docking operations of AUVs. Here, using a single quadrant photodiode mounted on an AUV, the optical detector was able to detect translational motion with respect to a light beacon mounted on the docking station [14].

This paper presents the second stage of the authors' study on leader-follower UUV formation using optical communication. After development of an analytical (numerical) simulator for the design of optical arrays for UUVs [15], the current focus of this study is on using optical distance detection algorithms to provide feedback to the vehicle control system. Here the feedback comes in the form of output imagers produced from the UUV light detector array.

## II. THEORETICAL BACKGROUND

The authors' simulator was developed based on ocean optics concepts, where a point source light field was used as a guiding beacon. The performance of the light detector array was evaluated for a variety of array geometries and a range of oceanic conditions (e.g. diffuse attenuation coefficients). The detector array performance was evaluated based upon its effectiveness to decouple distance and orientation changes of the sensor system with respect to a light source beacon. In this study, detection and control algorithms were developed based on the planar array to be

used to control the relative position and orientation of the UUVs. The hardware configuration is such that one UUV has a point light source at its crest (at the aft) and the other UUV has a light detector array mounted at its bow. The detection algorithms used for the control system are based on a number of key image properties that can be used to derive the critical degrees of freedom: 3 degrees-of-freedom (DOF) translation (i.e., along  $x$ ,  $y$  and  $z$ -axes) and 2-DOF rotation (i.e., yaw and pitch rotation). In this study, the UUVs are assumed to be stable about its roll axis ( $x$ -axis). Changes in distance and orientation between the UUVs are monitored using: 1) a classifier such as a Spectral Angle Mapper (SAM) [17] or Maximum Likelihood [18] based on a measure of resemblance between a reference image and an image under test and 2) changes in skewness of the image along a profile in the 2-D array. These key image properties that correspond to shifts in displacement and orientation between UUVs are compiled in a database of look up tables.

The success of the study was based on the ability of the control system to maintain a relative pose between the two UUVs (i.e., the leader and follower) to within an accuracy of  $\pm 0.1$  m in translation (i.e. in each  $x$ ,  $y$  and  $z$ -axes). This was accomplished by modeling the two vehicles and separately applying Proportional-Derivative (PD) control to each of the vehicles.

The control system of the UUV optical communication is mainly dependent on 1) the underwater optics and 2) UUV modeling and control design. The underwater optics is used to explain the underwater light field and its interaction with the detector array. The intensity of the light field produced by the light source is dominated mainly by its beam divergence and scattering. In the analytical studies in this paper, a dynamic model of the UUV is used, in conjunction with the UUV control system design, to determine the resulting response of the UUV to the received pose feedback from the detector arrays (via the developed simulator). Here, the leader and the follower UUVs are selected to be UUVs with full 6-DOF motion capability. In addition, both vehicles are assumed to be identical.

#### A. Optical Theory

The light field produced from a light source can be modeled with different mathematical functions. In this study, the light field is modeled with a Gaussian function as follows:

$$I(\theta) = A * \exp\left(-\frac{\theta^2}{2\sigma^2}\right) \quad (1)$$

where  $\theta$  is the incidence angle,  $A$  is the Gaussian amplitude and  $\sigma$  is the cut-off angle that limits the light emitting angle in its travel directions.

The intensity of the light beam is determined by ocean optic laws. One is the Inverse-Square Law, in which light intensity is inversely proportional to the inverse square of the distance:

$$I = \frac{S}{4\pi r^2} \quad (2)$$

where  $I$  is the intensity,  $r$  is the distance from the light source to the target, and  $S$  is the light intensity at the source.

Accordingly, the light intensity ratio at two different locations along the same axis can be described as:

$$\frac{I_1}{I_2} = \frac{\frac{S}{4\pi r_1^2}}{\frac{S}{4\pi r_2^2}} = \left(\frac{r_2^2}{r_1^2}\right) \quad (3)$$

The light field emitted from the leader vehicle is assumed to show uniform illumination characteristics and such that its intensity is not absorbed by the medium. The Inverse-Square Law represents the dominant source of light attenuation in water.

In addition to the expansion of the light beam, scattering along the light path also reduces light intensity. This is described by Beer's Law in which light intensity attenuates exponentially with distance based on the water clarity [16]. The amount of attenuation depends on the distance,  $z$ , from the light source and the attenuation coefficient,  $K$ , and is described as follows:

$$L(z; \hat{\xi}) = L(0; \hat{\xi})e^{(-Kz)} \quad (4)$$

where  $L$  denotes the radiance and  $\hat{\xi}$  is the directional vector. The diffuse attenuation factor in this study is  $0.0938 \text{ m}^{-1}$  and was determined from experiments conducted in the underwater facilities at University of New Hampshire.

#### B. UUV Modeling and Control

a) *UUV Modeling*: The UUV dynamic (kinetic and kinematics) are typically analyzed by using Newton's second law as in [19] and are presented here.

$$\tau = M\dot{v} + C(v)v + D(v)v + g(\eta) \quad (5)$$

The linear and angular velocity vector are represented in the body coordinate reference frame  $v \in \mathfrak{R}^{6 \times 1}$ . The UUV's mass and the hydrodynamic added mass derivatives are composed from the rigid body mass,  $M_{RB}$ , and the added mass matrix,  $M_A$ , (i.e.  $M = M_{RB} + M_A$ ). The Coriolis and the centripetal forces are described as  $C(v) = C_{RB}(v) + C_A(v)$ , where  $C_{RB}(v)$  and  $C_A(v)$  are derived from  $M_{RB}$  and  $M_A$  matrices, respectively. The UUV is also subjected to gravitational forces and moments,  $g(\eta)$ , as a function position and attitude in the Earth-fixed reference frame,  $\eta \in \mathfrak{R}^{6 \times 1}$ . Lastly, the quadratic damping force on the UUV  $D(v)$  that are described by following matrix.

$$D(v)v = \begin{bmatrix} v^T D_1 v \\ v^T D_2 v \\ v^T D_3 v \\ v^T D_4 v \\ v^T D_5 v \\ v^T D_6 v \end{bmatrix} \quad (6)$$

where  $D_i \in \mathfrak{R}^{6 \times 6}$  is a function of water density, drag coefficient, and projected cross-sectional area. The control input vector is derived with respect to the body coordinate frame, as the control input is applied to the body. The body-fixed reference frame is transformed into the Earth-fixed reference frame:

$$\eta_1 = J_1(\eta_2)v_1 \quad (7)$$

where  $\eta = [x \ y \ z \ \phi \ \theta \ \psi]^T$  is composed of translation along the  $x$ ,  $y$  and  $z$  axes and roll,  $\phi$ , pitch,  $\theta$ , and yaw,  $\psi$ , rotations defined in Earth-fixed coordinates. Here,  $\eta \in \mathfrak{R}^{6 \times 1}$  is the position and attitude state vector in the Earth-fixed coordinate frame, i.e.  $= [\eta_1 \ \eta_2]^T$ , where  $\eta_1 \in \mathfrak{R}^{3 \times 1}$  corresponds to translational motion in the Earth-fixed reference frame and  $\eta_2 = [\psi \ \theta \ \phi]^T$  is the vector of Euler angles (using a 3-2-1 rotation sequence) representing the vehicle attitude.  $J_1(\eta_2)$  is the transformation matrix (from the body fixed coordinates to Earth-fixed coordinates) and is described as

$$J_1(\eta_2) = \begin{bmatrix} c\psi c\theta & -s\psi c\phi + c\psi s\theta s\phi & s\psi s\phi + c\psi c\phi s\theta \\ s\psi c\theta & c\psi c\phi + s\psi s\theta s\phi & -c\psi s\phi + s\theta s\psi c\phi \\ -s\theta & c\theta s\phi & c\theta c\phi \end{bmatrix} \quad (8)$$

where  $s(\cdot)$  and  $c(\cdot)$  represents sine and cosine functions, respectively, while  $\phi$ ,  $\theta$  and  $\psi$  are the corresponding roll, pitch and yaw angles defined in Earth-fixed coordinates, respectively. As such, the corresponding attitude transformation matrix is an identity matrix such that  $J_1(\eta_2) = I_{3 \times 3}$ . Numerical integration of Eq. (8), therefore, results in the extraction of UUV position in the Earth-fixed coordinate frame.

*b) UUV Controller:* Under the assumption that the leader UUV has a known path *a priori*, the follower UUV can use information collected by the planar detector array as feedback to determine the leader UUV's relative pose:

$$\eta_f = \eta_l - \eta_d \quad (9)$$

where  $\eta_f$  is the follower pose,  $\eta_l$  is the leader pose determined by the follower, and  $\eta_d$  is the desired *relative* pose, incorporating desired relative distance and attitude, between the leader and the follower UUVs. The control problem in this case can be evaluated as both a point-to-point regulation problem and also as a trajectory control problem. The leader is given a reference input, i.e. step inputs, to travel to given waypoints while the follower generates its own time-varying trajectory from the leader motion. PD control of a nonlinear square system, as in Eq. (6), is shown to be asymptotically stable by using Lyapunov's Direct Method [12].

### III. EXPERIMENTAL DESIGN

#### A. Optical Parameters

The follower pose detection of the leader is based on the output image sampled by follower's detector consisting of an array of 21x21 detector elements. Specifically, the output image is the light field emitted from the leader's beacon that intersects with the planar detector array. The control algorithms in this study are tested using data produced from the detector array simulator previously developed by the authors. The input to the simulator is the relative pose geometry between the UUVs and the optical conditions of the medium. To extract the pose of the leader from the image, five main image parameters are used. These parameters are the Spectral Angle Mapper (SAM), the skewness of both the row and column of the resulting

intensity profile, and the row and column numbers of the image pixel with the highest intensity.

SAM is a measure of resemblance between a reference image and an image under test. Here, the reference image is the output obtained from the detector array when the light source and the detector have an offset along the  $x$ -axis only with no translation/rotation. The image under test is the output when there is a specific relative pose between the leader and the follower. SAM algorithm is given as:

$$\alpha = \cos^{-1} \left( \frac{\bar{U}_t \cdot \bar{V}_t}{\|\bar{U}_t\| \cdot \|\bar{V}_t\|} \right) \quad (13)$$

where  $\alpha$  is the SAM angle which varies between  $0^\circ$  and  $90^\circ$  and increases when the difference between the two images increases.  $\bar{U}_t$  and  $\bar{V}_t$  are the light intensity vectors obtained by the detectors for the reference image and image under test, respectively.

Two other key image parameters are the skewness values of the horizontal slope,  $Sk_x$ , and the vertical slope,  $Sk_y$ . The key in using these parameters is that they do not require significant computational effort. This is a key advantage, as the performance of the control system will degrade with increased computational delays.

Based on the location of the pixel with the maximum intensity, the horizontal and vertical gradients of the image are calculated. The use of the gradient of the intensities, rather than the intensity profile itself, is advantageous as the slope provides both directionality and asymmetry information. As an example, a reference image and sample detected image with the resulting horizontal and vertical profiles (showing the respective gradients in each direction) are provided in Fig. 1.

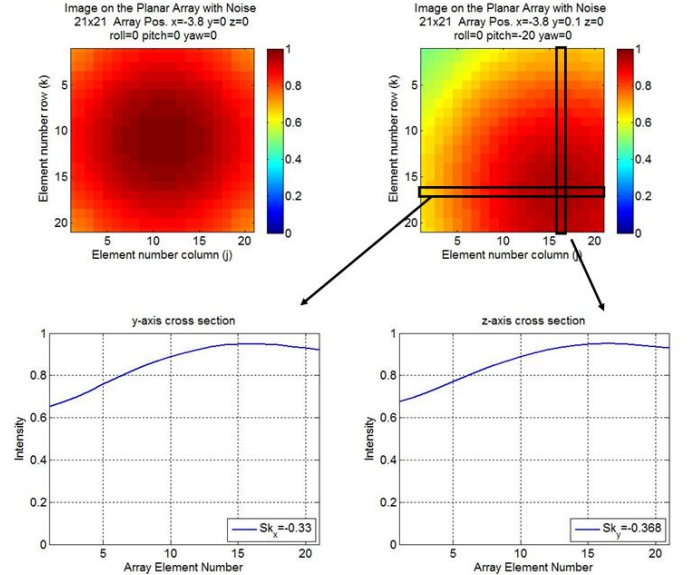


Fig. 1. Reference image and detected image. Reference image (top left), Detected image (top right), y-axis intensity profile (bottom left), z-axis intensity profile (bottom right).

#### B. Consolidated Data Base

Cases for varying geometries are simulated in the authors' numerical simulator. For translation motion, i.e.  $y$

and  $z$ -axis motions, the detector array is moved from  $-0.3\text{m}$  to  $0.3\text{m}$  at  $0.03\text{m}$  increments. For rotational motion, i.e. pitch and yaw motion, the follower is rotated from  $-30^\circ$  to  $30^\circ$  at  $3^\circ$  increments. The results from the simulations for each combination of motions are stored in a consolidated data base, in the form of a look up table. The table consists of the pose of the light source, i.e.  $x$ ,  $y$ ,  $z$ ,  $\psi$  (yaw) and  $\theta$  (pitch), the corresponding skewness values for the images, i.e.  $Sk_x$  and  $Sk_y$ ,  $\alpha$  (SAM angle), and the row and column number of the pixel with the highest intensity (Table I). Here, the first four columns indicate the inputs to the simulator (relative position between the light source and detector and the central pixel of the detector array). Columns five to column nine indicate the 5 chosen optical parameters describing the detected output.

TABLE I. A PORTION OF THE DATA BASE LOOK UP TABLE

INPUT				OUTPUT				
y (m)	z (m)	yaw (deg-rees)	pitch (deg-rees)	$Sk_x$	$Sk_y$	SAM (deg-rees)	Max row	Max col
0	0.03	24	3	-0.450	-0.040	6.55	10	18
0	0.03	24	6	-0.450	0.017	6.47	11	18
0	0.03	24	9	-0.456	0.072	6.48	12	18
0	0.03	24	12	-0.462	0.126	6.58	13	18
0	0.03	24	15	-0.465	0.185	6.75	14	18
0	0.03	24	18	-0.467	0.239	6.98	14	18
0	0.03	24	21	-0.477	0.293	7.26	15	18
0	0.03	24	24	-0.484	0.348	7.57	16	18

For this analytical study, the follower UUV detector array samples the incoming light field and the real-time measurements are compared to values contained in the aforementioned data base. After which, the leader UUV's relative pose is obtained. The leader UUV's pose parameters  $y$ ,  $z$ ,  $\theta$  and  $\psi$  are estimated using the compiled data base. The  $x$ -axis coordinate is estimated using the previously estimated  $y$ ,  $z$ ,  $\theta$  and  $\psi$ .

### C. Pose Detection Algorithm

The pose detection algorithm starts with the determination of the pixel (detector array element) with the greatest light intensity. Then, the poses that result in the same maximum pixel intensity location are extracted from the data base. (These poses are referred to as "candidate poses".) By looking at the intensity profile of the neighboring pixels to the pixel with the greatest intensity, any rotational (pitch and yaw) motion can be detected. Then, the skewness values ( $Sk_x$  and  $Sk_y$ ) and SAM angle are subtracted from the candidate pose parameters to obtain a "difference table". The result is a numerical cost function,  $P_i$ , comprised of the differences of the chosen optical parameters as a weighted sum:

$$P_i = c_1|Sk_x - Sk_{xi}| + c_2|Sk_y - Sk_{yi}| + c_3|SAM - SAM_i| \quad (14)$$

Here,  $P_i$ ,  $Sk_{xi}$ ,  $Sk_{yi}$  and  $SAM_i$  represent the penalty, skewness and SAM angle values, respectively, for the candidate pose,  $i$ . The parameters  $c_1$ ,  $c_2$  and  $c_3$  denote the respective weighting factors for row and column skewness and the SAM angle. Among the chosen candidate poses, the candidate with the lowest penalty score is chosen as the pose estimate.

The  $x$ -coordinate of the leader vehicle is estimated separately in a two-step procedure. In the first step, a rough estimate of the  $x$ -position is obtained based upon the total intensity of all of the detector array elements. A calibration procedure is performed by evaluating the intensities at  $x$ -coordinates from  $4\text{m}$  to  $8\text{m}$  at  $1\text{m}$  increments (Fig. 2). Here, the sum of intensities at the detector elements are calculated when the leader and the follower only have  $x$ -offset between them.

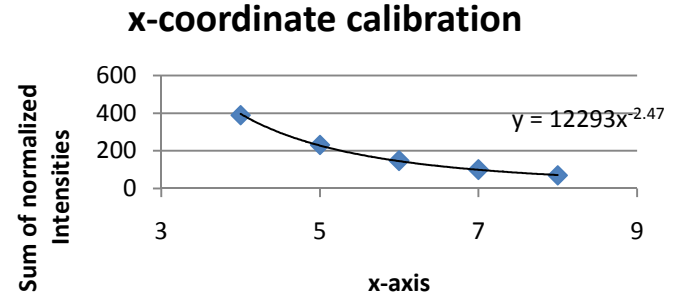


Fig. 2. –  $x$ - coordinate calibration plot.

The calibration curve results in the first  $x$ -coordinate estimation as follows

$$x_{est1} = 10^{\frac{\log_{10}(I_{total})}{-2.476}} \quad (15)$$

In the second step, the  $x$ -coordinate estimate from the previous step is corrected by using the estimated relative  $y$ ,  $z$ ,  $\theta$  (pitch) and  $\psi$  (yaw) values as follows:

$$x_{est} = x_{est1} - \sqrt{y_{est}^2 + z_{est}^2} - l \sin(\theta) \cos(\psi) \quad (16)$$

The estimated 5-DOF parameters are then used as feedback to the control system in order to perform the appropriate control action.

## IV. PRELIMINARY RESULTS

A preliminary analytical study is performed on a leader-follower UUV system. Both the leader and the follower vehicles are assumed to be identical with the same mass and inertia and both use the same PID control parameters (i.e.  $P=50$  and  $D=8$ ). (Here, a generic PID controller is used, without loss of generality, and to simply show proof of concept.) In addition, the leader UUV is given two reference points,  $R_1$  and  $R_2$  while the follower is required to maintain a relative  $x$ -offset of  $4\text{m}$  from the leader and to maintain  $y$ -axis alignment with the leader UUV (Table II). The leader is given step input changes, directed to travel to the specified waypoints. Initially, the leader UUV is commanded to go from its initial position of  $(4, 0)$  to  $R_1(4, 0.5)$ .

The control goal for the follower UUV is to follow the leader from 4m behind in  $x$ -axis direction while maintaining the same  $y$ -axis coordinate. The trajectories generated by the detection algorithms are smoothed using a Kalman filter as the distance detection algorithm results in a finite resolution, i.e. 0.03m in  $y$ - $z$  axes motion detection.

TABLE II. INITIAL POSITIONS, CONTROL GOALS AND RESULTS OF THE SIMULATION

	Initial Position (m) (x,y)	Desired Final Position (x,y)	Final Position (m) (x,y)	Desired Offset (m) (x,y)	Final Offset (m)	Controller Parameters
Leader UUV	(4,0)	(5,0.5)	(5.26,0.5)	$\Delta x_d=4$	$\Delta x_f=3.97$	P=50 D=8
Follower UUV	(0,0)	(1,0.5)	(1.29,0.55)	$\Delta y_d=0$	$\Delta y_f=0.05$	P=50 D=8

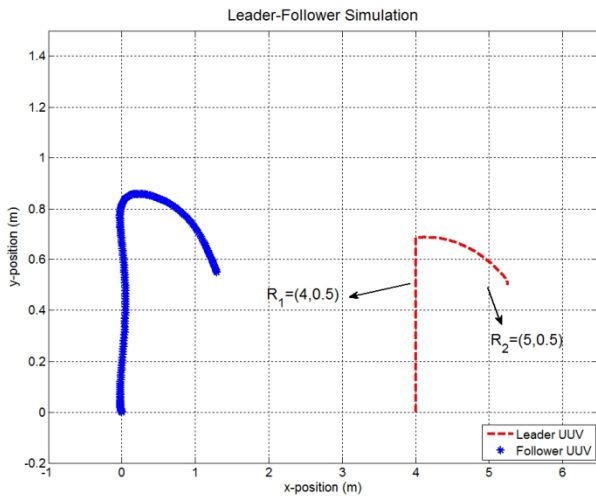


Fig. 3. Waypoints  $R_1$  and  $R_2$ , the leader (red dashed line) and the follower motions (blue stars) in  $xy$ -plane.

As shown in Fig. 3, the performance results of the leader-follower UUV system (i.e. detection algorithm and control design) demonstrate that the follower UUV maintains the desired fixed distance from the leader with acceptable accuracy. (The authors note that accuracy can also be increased with other control methods.) It is observed that the leader UUV does not deviate in the  $x$ -direction, but has an overshoot in the  $y$ -direction at the first waypoint. At the second waypoint, i.e.  $R_2$ , the leader's PID controller manages to eliminate the error in the  $y$ -direction but results in an overshoot in  $x$ -direction.

Contrary to the leader UUV, the follower UUV generates its own desired time-varying trajectory by observing and estimating the motion of the leader UUV. The reference trajectory generated by the follower UUV and smoothed by the Kalman filter results in a smoother trajectory than the trajectories generated by the detection algorithm, especially in  $y$ -axis.

Fig. 4 and Fig. 5 show the actual leader and follower motion in  $x$  and  $y$ -axes, respectively, the trajectory generated by the follower and the smoothed trajectory. Overall, the leader UUV completes its task with negligible

steady-state error in  $y$ -axis and 0.26m steady-state error in  $x$ -axis. The follower UUV manages to keep its distance with the leader UUV to 3.97m in the  $x$ -axis direction and 0.05m in the  $y$ -axis direction. The errors associated with the follower in the two axes are 0.03m and 0.05m, respectively and are within the tolerance of the pre-defined control goals.

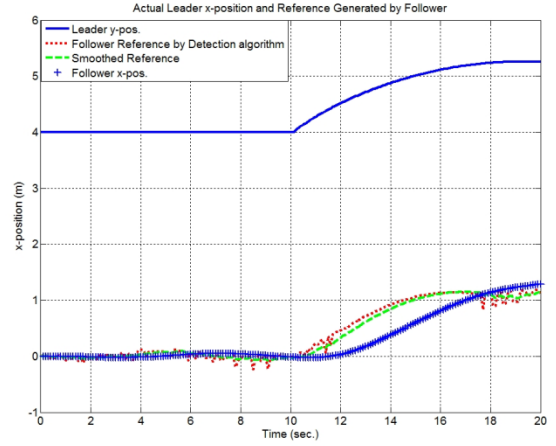


Fig. 4. The UUV time-varying  $x$ -axis coordinates: the leader UUV's  $x$ -axis motion (blue line), the follower reference trajectory generated by the detection algorithm results (red dots), and a smoothed trajectory (green line).

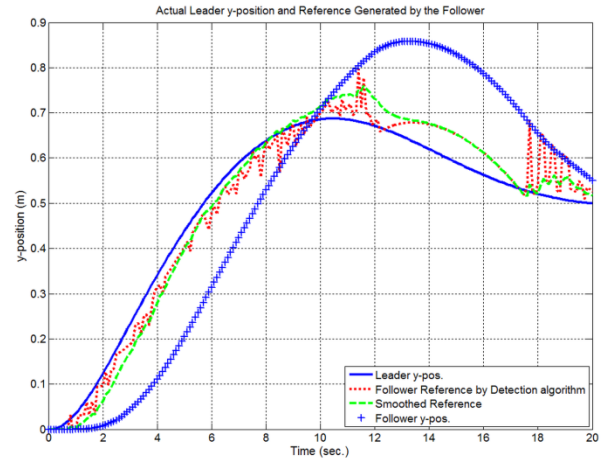


Fig. 5. The leader UUV's  $y$ -axis motion: the leader UUV's  $x$ -axis motion (blue line), the follower reference trajectory generated by the detection algorithm results (red dots), and a smoothed trajectory (green line)

## V. CONCLUSIONS

The goals of this study are to develop a detection algorithm and to analyze the resulting control system performance (using a generic PID controller) for a leader-follower UUV system using an optical communication detector array. The follower UUV is able to detect the motion of the leader UUV based on five parameters ( $Sk_x$ ,  $Sk_y$ , the row and column elements corresponding to a greatest light intensity, and the SAM angle) extracted from the output imagery of the detector array. A data base is constructed taking into account varying combinations of relative positions and orientations of the leader UUV with respect to the follower UUV. Based on a pre-defined course of the leader UUV, virtual real-time distance detection

algorithms are applied using the intensity measurements from the detector array and the data base look up tables. The leader motions are calculated based on row and column elements in the imagery that are taken as pose candidates. The final pose for the leader position is calculated based on a calculated cost function that incorporates the differences of the skewness of the beam in the imagery and corresponding SAM angles.

Preliminary results from simulations that include the leader UUV following two reference waypoints (as step inputs) demonstrate that the control system has good performance. The leader UUV control system manages to maintain the final control goal to within 5% overshoot in the  $x$ -axis direction with no overshoot in the  $y$ -axis direction. The follower UUV generates its trajectory based on the feedback received from the detection algorithm and using the Kalman filter to smooth the trajectory. The follower UUV is able to complete its control goal to within an accuracy of 0.03m in the  $x$ -axis direction and 0.05m in the  $y$ -axis direction. The follower UUV motion accuracy is dependent on the accuracy of its detection algorithm. Because the follower UUV generates its own time-varying trajectory, it is vital that the reference trajectory is smooth. To compensate for this time-varying trajectory, a Kalman filter is applied. Although the follower UUV performs well in maintaining its control goals (traveling to a way-point), better controllers could be implemented for increased tracking performance.

Future work includes developing a more advanced detection algorithm that is able to provide better motion detection capability. Also, observed cross-talk during the simulations, e.g. detection of yaw and pitch motion when the leader's trajectory did not include any rotation, is to be minimized. Furthermore, the PD controller performs well in point-to-point control problems, but is not sufficient in the trajectory following aspects of the simulations. Therefore, the implemented control algorithm should also be improved, especially that of the follower UUV, perhaps using more sophisticated controllers specifically designed for nonlinear systems.

#### ACKNOWLEDGEMENTS

This project was funded by the University of New Hampshire and the LINK Foundation Fellowship for Ocean Engineering.

#### REFERENCES

- [1] H. J. Curti, G. G. Acosta and O. A. Calvo, "Autonomous underwater pipeline inspection in autotracker project: the simulation module," *In Proc. of IEEE/OCEANS'05 Europe Conf.*, Jun. 21-23 Brest, France vol. 1, pp 384-388. DOI: [10.1109/OCEANSE.2005.1511745](https://doi.org/10.1109/OCEANSE.2005.1511745)
- [2] G. Inglis, C. Smart, I. Vaughn and C. Roman, "A pipeline for structured light bathymetric mapping," *in Proc. of International Conference on Intelligent Robots and Systems (IROS) 2012*, Oct. 7-12, Vilamoura, Algarve, Portugal pp. 4425-4432, DOI: [10.1109/IROS.2012.6386038](https://doi.org/10.1109/IROS.2012.6386038)
- [3] J. Jalbert, J. Baker, J. Duchesney, P. Pietryka, W. Dalton, D.R. Blidberg, S. Chappell, R. Nitzel and K. Holappa, "A solar-powered autonomous underwater vehicle," *in Proc. of OCEANS*, 2003, vol. 2, pp. 1132 - 1140.
- [4] M. Hamilton., S. Kemna, and D. T. Hughes, "Antisubmarine warfare applications for autonomous underwater vehicles: the GLINT09 field trial results," *Journal of Field Robotics*, vol. 27, No.6, pp. 890-902, 2010.

- [5] Y. Zhang and H. Mehrjerdi, "A survey on multiple unmanned vehicles formation control and coordination: normal and fault situations," *IEEE Conf. on Unmanned Aircraft Systems*, pp. 1087-1096, 2013
- [6] J. P. Desai, J. Ostrowski, and V. Kumar, "Controlling formations of multiple mobile robots," *in Proc. IEEE Int. Conf. on Robotics and Automation*, 1998, pp. 2864-2869.
- [7] B. Jouvencel, O. Parodi, and X. Xiang, "Coordinated formation control of multiple autonomous underwater vehicles for pipeline inspection," *in International Journal of Advanced Robotic Systems*, 7(1), pg. 75-84, 2010.
- [8] P. Calado and J. Sousa, "Leader-follower control of underwater vehicles over acoustic communications," *in OCEANS, 2011 IEEE - Spain*, June 2011, pp. 1-6
- [9] P. Feng, "Leader-follower cooperative navigation with communication delays for multi AUVs," *Proceedings of the IEEE International Conference on Signal Processing, Communications and Computing (ICSPCC)*, Xi'an, China, 2011.
- [10] D. B. Edwards, T. A. Bean, D. L. Odell and M. J. Anderson, "A leader-follower algorithm for multiple AUV formations," *in Proc. IEEE/OES Autonomous Underwater Vehicles*, Sebasco Estates, ME, 2004, pp. 517-523, DOI: [10.1109/AUV.2004.1431191](https://doi.org/10.1109/AUV.2004.1431191).
- [11] I. Vasilescu, P. Varshavskaya, K. Kotay, and D. Rus, "Autonomous modular optical underwater robot (AMOUR) design, prototype and feasibility study," *in International Conference on Robotics and Automation*, Barcelona, Spain, 18-22 Apr., 2005 DOI: [10.1109/ROBOT.2005.1570343](https://doi.org/10.1109/ROBOT.2005.1570343).
- [12] F. Eren, M. W. Thein, B. Celikkol, J. DeCew and S. Pe'eri, "Distance detection of unmanned underwater vehicles by utilizing optical sensor feedback in a leader-follower formation," *in Proc. IEEE/MTS OCEANS Conf.*, Hampton Road, VA, 2012. DOI: [10.1109/OCEANS.2012.6404934](https://doi.org/10.1109/OCEANS.2012.6404934)
- [13] F. Eren, S. Pe'eri, M. W. Thein, "Characterization of optical communication in a leader-follower unmanned underwater vehicle formation," *in Proc. SPIE, Ocean Sensing and Monitoring V*, vol. 8726, 2013.
- [14] S. Cowen, S. Briest and J. Dombrowski, "Underwater Docking of autonomous undersea vehicles using optical terminal guidance," *in Proc. IEEE OCEANS Conf.*, Oct. 1997, vol. 2, pp. 1143-1147.
- [15] F. Eren, S. Pe'eri, Y. Rzhanov, M. Thein and B. Celikkol, "Detector Array Design for Optical Sensor Based Pose Detection between Unmanned Underwater Vehicles (UUVs)," unpublished.
- [16] C. Mobley, *Light and Water*, Academic Press Inc., 1994.
- [17] F. A. Kruse, A. B. Lefkoff, J. B. Boardman, K. B. Heidebrecht, A. T. Shapiro, P. J. Barloon, and A. F. H. Goetz, "The spectral image processing system (SIPS) - Interactive visualization and analysis of imaging spectrometer data," *Remote sensing of environment*, vol. 44, no. 2, pp. 145- 163, 1993.
- [18] W. Wei and J. M. Mendel, "Maximum-likelihood classification for digital amplitude-phase modulations," *IEEE Trans. Commun.*, vol. 48, no.2, pp. 189-193, Feb. 2000
- [19] T. I. Fossen, *Guidance and Control of Ocean Vehicles*, Wiley & Sons Ltd., 1994.